 

*Accounts*

# Fluorescence Probe Method for Investigating Polymer Structures in Nanometer Dimensions

**Shinzaburo Ito* and Hiroyuki Aoki**

Department of Polymer Chemistry, Graduate School of Engineering, Kyoto University, Sakyo, Kyoto 606-8501

Received March 12, 2003; E-mail: sito@photo.polym.kyoto-u.ac.jp

The applications of the optical methods using fluorescent probes for investigating polymer structure and dynamics at a molecular level are reviewed. The versatile and particular abilities of the fluorescence method have been exemplified using ultrathin films made of polymer monolayers, which provided fine model systems designed with a nanometer precision. In the latter part of this article, the emerging research field of scanning near-field optical microscopy (SNOM) is introduced. This novel microscopic technique enabled us to carry out spectroscopic and time-resolved measurements with a lateral resolution of 100 nm, which is obviously beyond the diffraction limit of light. We applied SNOM to study various nanometer-scale structures of polymer assemblies, such as the two-dimensional phase separation structure, morphology of single polymer chains, and structural inhomogeneity of polymer networks. These results showed that the combination of the fluorescence method and SNOM technique will open a new field of research on polymeric materials by providing molecular information on the basis of real optical images on a nanometric scale.

Polymers are indispensable building blocks for constructing molecular architectures with various functionalities. A typical example is found in biopolymers such as cellulose, proteins, and enzymes, in which the well-defined primary structure of component polymers unequivocally determines the highly ordered structure of living things, yielding the elaborated biological functions all at once. This example clearly indicates that the formation of fine structures in consecutive dimensions from a nanometer to a hundred nanometers plays a critical role in designing functionality of materials. Therefore, novel techniques for fabrication and analysis of nano-structures have been widely explored, and some of them have made rapid progress in the last decade. Recent developments in analytical tools such as X-ray, NMR, AFM, and TEM, have enabled us to view the molecular structures in nanometer dimensions, and the information thus obtained has been again utilized for making nano-structures of materials. Among these analytical techniques, the fluorescence probe method has made on outstanding contribution as an advanced technology providing high resolutions in both temporal and spatial regions. A fluorescent probe incorporated into a specimen can provide various types of molecular information about the surroundings and the molecule itself, such as molecular motion, orientation, conformation, distribution, polarity, viscosity etc,[1–3] most of which are never obtainable by other techniques. Therefore, the fluorescence probe method has a large potential for a variety of applications in chemistry, biology, and medical uses. Among its versatile applications, this paper will focus on investigations of the structure of polymeric materials in nanometer dimensions. First, the advantages of this method are described briefly and then the recent developments for structural researches will be discussed, using mainly scanning near-field optical microscopy and ultrathin polymer films: the former microscopy gives a superb lateral resolution to the fluorescence method[4,5] and the latter polymer films provide excellent model systems having well-defined nano-structures.[6–10]

## 1. Characteristics of the Fluorescence Method

**1.1. Sensitivity in Detection.** In principle, physical and chemical properties of bulk materials result from characteristics of the molecular ensemble on average over the volume of observation. Therefore, in order to clarify the origin of materials' functions, there is always strong demand for researchers to investigate a very small specific local area, e.g., detection of signals from the genuine surface,[11] the interior of a micelle,[12] a cluster of molecules,[13,14] and even from a single molecule as an extreme case.[15–17] It is easily imaginable that the apparatus should have high enough sensitivity to detect weak signals from these samples containing a limited number of molecules in a small space.

The photon is a quantum unit carrying both information and energy in the form of electro-magnetic waves. One of the particular advantages of the fluorescence method lies in the remarkably high sensitivity in detecting light. Under the present circumstances of advanced technology, it is quite easy to detect a single photon by a photo-multiplier or a photodiode with a quantum yield larger than 40–60 percent. This means that we are able to address each molecule and take out data from

Published on the web September 15, 2003; DOI 10.1246/bcsj.76.1693

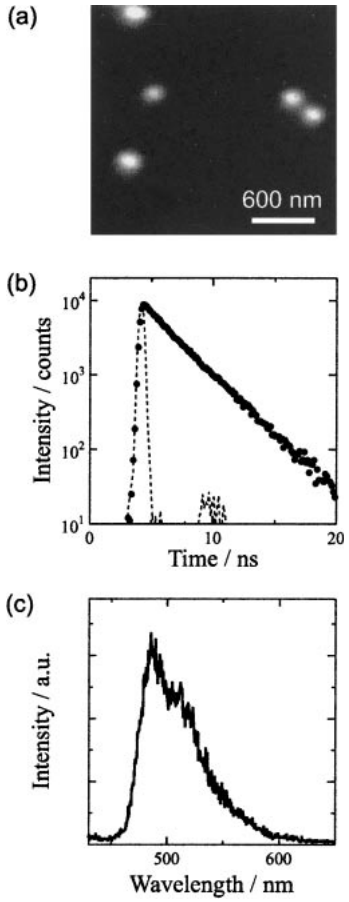


Fig. 1. (a) Fluorescence image of polystyrene latex particles labeled with fluorescent dyes (Polysciences, Inc., Fluoresbrite:YG-0.10). The excitation wavelength was 442 nm and the fluorescence was detected through long-pass filters. (b) A fluorescence decay curve observed for a certain particle in (a). The picosecond pulsed light at 410 nm from a Ti:Sapphire laser was used for excitation. (c) Fluorescence spectrum for the particle excited at 410 nm.

the molecule. Figure 1 shows the photon counting data for a polystyrene latex particle (Polysciences, Inc.) with a diameter of 100 nm, which is labeled with fluorescent dyes. Although one particle contains only about a hundred dyes within the tiny volume of $2 \times 10^{-3}$ $\mu m^3$, the fluorescence decay (b) and the fluorescence spectrum (c) can be measured with sufficient intensity using an optical microscope and a photon counting system. There exists no alternative method to analyze the chemicals and dynamics of such a small object. Another example is found in many works on Langmuir–Blodgett films, which provide specimens of a monolayer containing fluorescent dyes within a thickness of 1 nm. Even if the fraction of chromophoric units is reduced to less than 1/1000 of the constituent units of the monolayer, the fluorescence spectra can be observed from the small number of chromophores existing in the extremely thin film.[18–20] Thus, the fluorescence method is a highly sensitive method applicable to a wide range of nanoscale technology and science.

**1.2. Molecular Probe.** Many fluorescent probes have been synthesized and commercialized as labeling reagents for use in chromatography and microscopy. Most of which are composed of a chromophoric unit and a substituent reactive to a specific chemical group of the specimen. These probes act as an indicator of the object materials on the chromatogram and in the microscopic images. This site-selective labeling of the molecules of interest is one of the particular characteristics of the fluorescence method. As for polymer labeling, living polymerization is a very effective manner in order to selectively introduce fluorescent chromophores into a desired part of the polymer chain. Figure 2(a) depicts some chemical structures of labeled polymers in which an anthracene probe is introduced at the chain center or at the chain end, using termination of living anionic polymerization with chromophoric bromide.[21,22] In this example, anthracene was employed because it has a well-defined transition dipole moment, the direction being parallel to the short axis of the aromatic rings; therefore, the absorption and fluorescence transitions take place preferentially for the polarized light whose electric field orients parallel to the transition dipole, i.e., to the direction of the polymer chain. The measurement of time-resolved fluorescence depolarization directly provides the auto-correlation function for the orientation of transition dipole; consequently, the dynamics of the chain center and the chain end are obtained as a function of temperature, solvent viscosity, segment density, molecular weight and so on.[23–25] In Fig. 2(a), 9,10-bis(bromomethyl)anthracence and 9-(bromomethyl)anthracene were coupled with the living anionic end of the polymers, resulting in labeled chains exactly at the center and the end of the polymers, respectively, whose molecular weight can be controlled within a low dispersion of molecular weight by living polymerization technique. Similar to this, living cationic polymerization and living radical polymerization have been also utilized as a labeling method, as shown in Figs. 2(b) and 2(c).[26] In particular, the living radical polymerization recently developed by a few research groups has opened a wide range of possibilities for labeling,[27,28] because this novel technique is applicable to many kinds of monomers, and because the living radicals (dormant radicals) are relatively inactive compared with the high reactivity of anionic species. Since fluorescent chromophores have, in general, low ionization potential and large electron affinity, only a few kinds of probes are stable against the anionic living end; therefore, very few chromophores had been employed so far as a labeling reagent.

Owing to these labeling techniques, physical and chemical functions of a specific part of polymers can be visualized at a molecular level. For example, the interfaces of styrene-isoprene block copolymers were probed during the course of micro-phase separation by using phenanthrene and anthracene probes, which were introduced exactly at the covalent linkage between two block chains.[29,30] Thus, the elaborate labeling technique is another key point for successful observation, and the uniqueness of the fluorescence method can be further exemplified in precise syntheses of polymers.

**1.3. Spectroscopic Analysis.** Analysis of fluorescence spectra gives rise to various forms of information about molecules. Let us consider two cases, unimolecular and bimolecular phenomena, that may alter the fluorescence spectra. First, a unimolecular probe is often used for studying the local

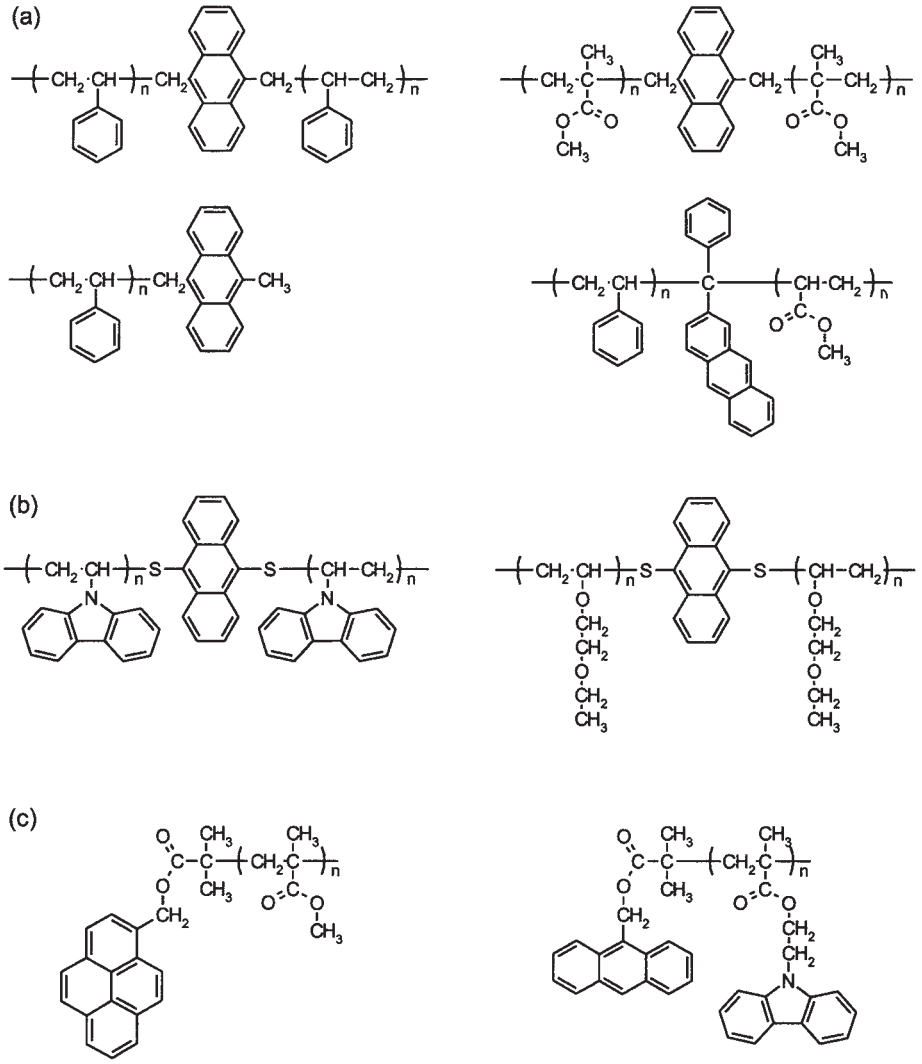


Fig. 2. Chemical structure of polymer samples labeled (a) by termination of anionic polymerization with chromophoric bromide, (b) by cationic polymerization, and (c) by living radical polymerization with a chromophoric initiator.

polarity of samples. It is well known that the excited state of a molecule has a polarity much larger than its ground state. Furthermore, if an electron-donating unit and an electron-accepting unit are substituted to a conjugated system like an aromatic ring, the unsymmetrical distribution of electrons induces strong intramolecular charge transfer in the excited state. The large dipole moment generated between separated charges is more stabilized with the increase of polarity of the surrounding solvents. Consequently, the higher the polarity of solvent, the longer the emission wavelength observed. Thus, the fluorescence spectrum is indicative of the micro-polarity of the medium. Morishima et al. studied the unimolecular polymeric micelle (unimer) formed by amphiphilic polymers in aqueous solutions; the physical constants such as hydrodynamic radii and aggregation number of micelles were evaluated from the fluorescence spectra of probes.[31,32] Iwai et al. reported a phase transition of poly(*N*-isopropylacrylamide) gel, which was monitored by a steep change in the emission wavelength at the transition temperature of the gel.[33] These are just a few of the many spectroscopic studies using fluorescent polarity probes.

As to bimolecular interactions, excimer formation and energy transfer phenomena lead to marked alteration of fluorescence spectra; these two phenomena have often been utilized for probing the degree of interaction between two molecules. An excimer is an encounter complex (excited dimer) composed of two molecules of the same kind, and its broad emission appears as a new band at the wavelength longer than that of monomer fluorescence from an isolated molecule. Since the formation kinetics depends on the mutual diffusion of corresponding molecules, the appearance of excimer emission becomes a good measure of Brownian motion, local concentration, and collisional frequency of molecules.[34–36] An excimer is stabilized only in the excited state by the exciton resonance and charge transfer interactions, those effective over a short distance of a few angstroms. Therefore, the excimer is formed not only in the liquid phase through mutual diffusion, but also in a solid matrix, if two molecules are placed close to each other, within a short interaction distance. The excimer fluorescence from polymer films has been used for probing the degree of aggregation of molecules. For example, vinyl aromatic polymers, in general, show excimer emission as the major

component of fluorescence spectra. Frank et al. reported examples where the compatibility of polymer blends could be monitored by the formation efficiency of excimer.[37,38] The other bimolecular interaction, energy transfer, is the most powerful tool for investigating nano-structures of polymers. Liu et al. named this method as a "spectroscopic nano-ruler".[39,40] The details will be described later in section 2.

**1.4. Time-Domain Resolution.** It should be noted that the fluorescence method has another remarkable advantage, that is, the time-resolving ability. The growing laser technology has enabled us to generate ultra-short pulsed light in the picosecond or femtosecond time region. Nowadays, such a pulsed laser system is widely used in combination with a high speed detector such as a microchannel plate photomultiplier and a streak camera system equipped with a monochromator. These advanced instruments provide sufficient picosecond time-resolution, while most of the fluorescent dyes have lifetimes of a few nanoseconds. Therefore, the dynamics of molecular motion and excitation kinetics including intra- and inter-molecular processes can be easily investigated. The detailed energy dissipation processes, both photophysical and photochemical, can be analyzed through the quantitative evaluation of individual rate constants closely related to structures of polymer systems. A good example will be presented in the next section.

## 2. Energy Transfer Method as a Spectroscopic Nano-Ruler

Energy transfer through the dipole–dipole interaction (Foerster mechanism) has been well characterized theoretically and experimentally. Therefore, many researchers have employed this phenomenon as a nano-scale ruler in order to evaluate the distance of separation between energy donor (D) and acceptor (A) molecules, which are labeled at specific positions. According to the Foerster theory,[41] the energy transfer rate constant $k_{ij}$ from a certain donor $D_i$ to an acceptor $A_j$ is given by

$$k_{ij} = (R_0/r_{ij})^6/\tau_D \quad (1)$$

where $r_{ij}$ is the distance between $D_i$ and $A_j$; and $R_0$ is the critical transfer radius at which the energy transfer rate constant from D becomes equal to the intrinsic decay rate, $1/\tau_D$. $R_0$ is given by the overlap of the absorption spectrum of A and the fluorescence spectrum of D. For example, phenanthrene as D and anthracene as A are known as a preferable pair for the energy transfer experiments, and the $R_0$ of this pair is evaluated as 2.1 nm. This means that the rate constant $k_{ij}$ will change steeply at distances of around a few nanometers. Consequently, we are able to estimate $r_{ij}$ through the observation of energy transfer efficiency or directly from the rate constant $k_{ij}$.

This spectroscopic technique can be applied to characterization of the layered structure of ultrathin films made of poly(vinyl octanal acetal) (PVO).[42] Figure 3 depicts chemical structures of PVO and PVO polymers labeled separately with D and A. The adequate balance of hydrophobic and hydrophilic parts of PVO makes it a stable monolayer on the water surface,[43,44] and the monolayer could be deposited layer-by-layer on a quartz plate with an arbitrary order and an arbitrary number, yielding nano-structured ultrathin film with a thickness of

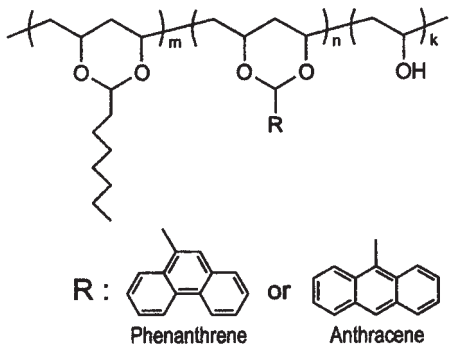


Fig. 3. Chemical structure of poly(vinyl octanal acetal) (PVO) and fluorescent D and A labels introduced to the side chain.

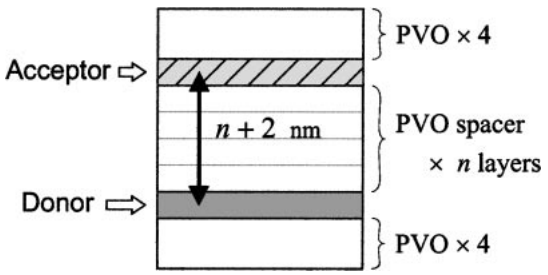


Fig. 4. Layered structure of polymer films prepared for the energy transfer experiment, in which the distance between the donor and acceptor layers are changed with *n* layers of PVO.

only 1 nm per layer. Due to the thinness of the multi-layered film, however, there is really no effective method besides the energy transfer technique for characterizing the nano-structure inside the thin film. The energy transfer measurement is able to verify whether the distance between two layers is made exactly at a given distance as designed by the deposition sequence. Figure 4 illustrates the layered structure of polymer films prepared for the energy transfer experiment. The multi-layered films, abbreviated as D*n*A, were fabricated on a quartz plate in the following sequence: 1) PVO layers for the precoating layer without chromophores, 2) two layers of PVO labeled with D, 3) *n* layers of PVO for the spacer between D and A layers, 4) two layers of PVO labeled with A, and again 5) PVO layers for the protecting layers. Since the layer thickness of PVO is only 1 nm, the distance between D and A layers must be $n + 2$ nm on average and this separation was proved by the energy transfer technique. As seen in Fig. 5, the fluorescence spectra of D*n*A films drastically changed in intensity at the D and A emission bands; the intensity of D fluorescence at 350 nm decreased, while the intensity of A at 400 nm significantly increased with the decrease of spacing, *n*. This means that the shorter the separation distance between D–A layers, the higher the energy transfer efficiency observed. Although this result indicated successful control of energy transfer processes, time-resolved experiments are highly needed to quantitatively discuss the nano-structure.

Figure 6 depicts the schematic illustration for the present system in which D and A molecules are distributed randomly in a plane but placed in the specific layers as designed. The

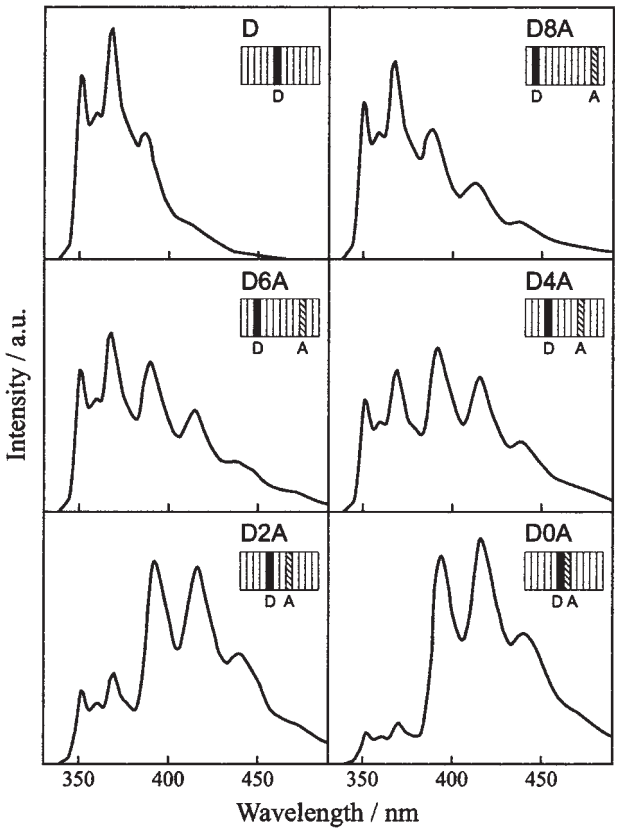


Fig. 5. Fluorescence spectra of D*n*A films. The inset of each figure shows the layer structure. The energy donor (phenanthrene) was excited at 298 nm.[42]

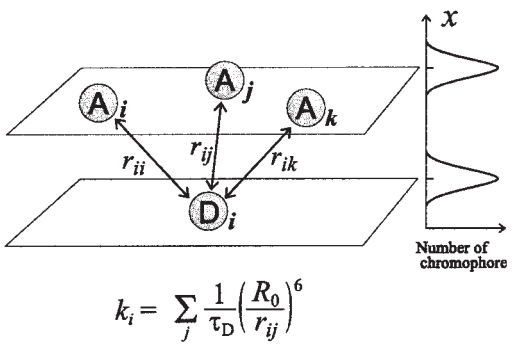


Fig. 6. Illustration for the donor and acceptor probes locating in the corresponding polymer monolayer. The separation distances and displacement were calculated according to the Gaussian distribution.

energy transfer rate constant from $D_i$ to all of A chromophores on the neighboring A layers is presented by the sum of Eq. 1.

$$k_i = (1/\tau_D)\sum_j (R_0/r_{ij})^6 \quad (2)$$

Therefore, the survival probability $p_i(t)$ of the excited $D_i$ at a time $t$ is given as follows:

$$p_i(t) = \exp(-t/\tau_D - k_i t) \quad (3)$$

Experimentally observed probability $p(t)$ of D is calculated by the average of $p_i(t)$ over all donor molecules:

$$p(t) = (1/n_D)\sum_i p_i(t) \quad (4)$$

where $n_D$ is the number of donors on the D layer, and $p(t)$ in Eq. 4 corresponds to the fluorescence decay curve. Integration of Eq. 4 gives the fluorescence quantum yield $q_D$ under the steady state excitation,

$$q_D = k_f \int p(t)\mathrm{d}t \quad (5)$$

where $k_f$ is the emission probability of the excited D unit. All of these equations 1–5 are numerically calculated with $r_{ij}$ for a given coordinate of D and A chromophores; these chromophores were generated on a computer according to the expected layer structure using appropriate distribution functions. For example, a Gaussian function is the most appropriate distribution function:

$$c(x) = (c_0/\sigma(2\pi)^{1/2})\exp(-(x - x_0)^2/2\sigma^2) \quad (6)$$

where $c(x)$ is the concentration of chromophores at the displacement $x$, and $\sigma^2$ is the variance of distribution. Therefore, the analyses of energy transfer efficiency and decay kinetics for the D molecules provide quantitative values of the distance and its distribution of molecules in a nanometer scale. This outlook is schematically illustrated in Fig. 6, where D and A chromophores were placed, by Eq. 6, along the direction of film thickness. All of these procedures were performed repeatedly and statistically using a computer.

Figure 7 shows fluorescence decay curves of D4A, D6A, and D8A films. Although each decay curve looks like a single-component exponential function, it obviously contains shorter decay components at the early stage compared to the later part of the decay curve. It should be a single exponential function, if each layer is perfectly fixed at the given plane and all D and A chromophores have the same circumstances between two layers, as schematically shown in Fig. 4. This is not true because the deposition was done by Y-type (double layers deposited in both the down and the up strokes of dipping) and it is known that a slight rearrangement of structures takes place after the deposition. This effective thickness of the labeled layers and the structural relaxation give rise to a distance distribution of chromophores in the direction of film thickness as shown in Fig. 6, and the variation of distance results in the multi-component decay kinetics of each D molecule; the shorter decay components at the early stage indicate the smaller separation of D–A molecules, and the longer decay components at the later stage show the larger separation of D–A molecules compared with the layer distance. Figure 7 (top) shows the distribution of chromophores evaluated by the decay analysis. The abscissa indicates the displacement $x$ in nm unit. The DA chromophores were expected to be at the positions of broken lines, but the energy transfer analysis tells us that, in a real system, they were distributed in a Gaussian form with standard deviations $\sigma$ of 1.3–2.2 nm around the positions expected from the layer thickness.

It is worth noting that this analysis can also be used for investigating the inter-layer diffusion process of chromophores by monitoring time-dependent distribution functions as follows:[45,46]

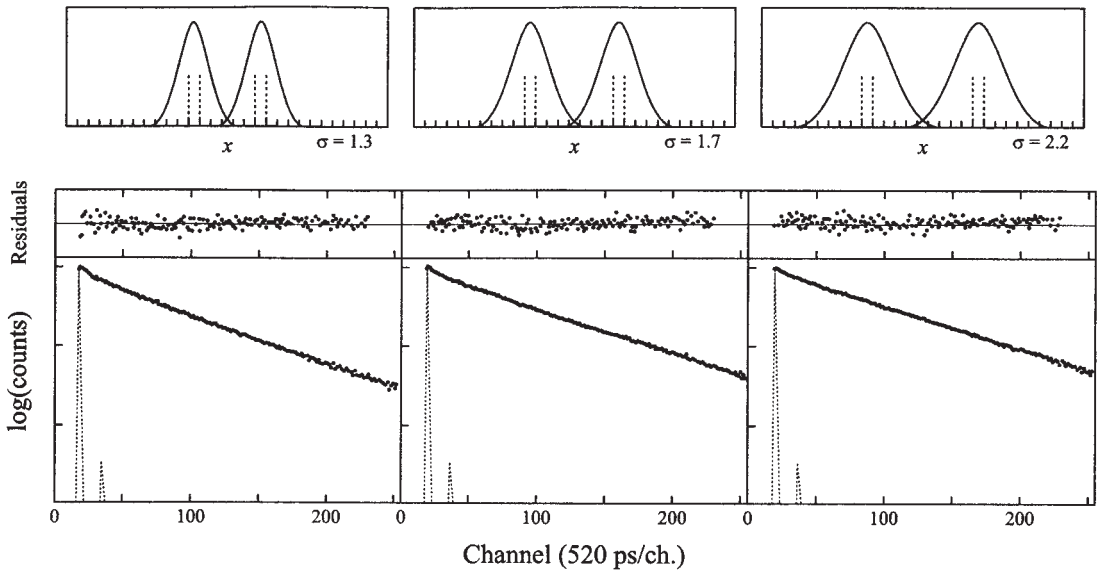


Fig. 7. Fluorescence decay curves for D4A (left), D6A (middle), and D8A (right) and the residual plots for the best fit curves based on the Foerster kinetics and the distribution function. The donor was excited with pulsed laser light at 298 nm, and the fluorescence decay was measured at 350–360 nm. The upper figures show the distribution of donor and acceptor probes and their standard deviation in nm unit. The broken lines show the positions of D and A chromophores for the perfect layer structure expected from the deposition sequence.[42]

$$\sigma^2 = 2Dt + {\sigma_0}^2 \tag{7}$$

where $D$ is the diffusion constant of chromophores attached to the polymer segment, and ${\sigma_0}^2$ is the initial dispersion at $t = 0$. Under elevated temperatures higher than the glass transition temperature $T_g$ of PVO, the polymer chains in each layer are allowed to change their conformation, resulting in relaxation of the layered structure. This phenomenon was monitored by the energy transfer experiments at various temperatures, and analyzed with Eqs. 6 and 7. The diffusion constants of polymer segments thus obtained showed very low activation energy $E_a$ for the structural relaxation of these multi-layer films. These values $D$ and $E_a$ gave clear evidence for the particular relaxation mechanism, i.e., "entropy relaxation" of ultrathin polymer films, which occurs by segmental motion of polymer chains from a 2-dimensionally restricted conformation to a 3-dimensionally random conformation.[47,48] These examples indicate that the energy transfer method actually acts as a spectroscopic nano-ruler; thus, they show that it is a unique and powerful tool for investigating nano-structures and dynamic processes in an organized molecular system.

## 3. Microscopic Imaging of Nanometric Structures

**3.1. Outlook of SNOM.** The scanning probe microscope invented in the early 1980s has been greatly improved during the last decade and has brought significant contributions to surface science and material science. Many kinds of scanning probe microscopes based on different types of interactions between the probe tip and the surface have been developed. Scanning Near Field Optical Microscope (SNOM) is one such microscope.[4,5] It is an optical microscope, but has a high spatial resolution beyond the diffraction limit of light. The probe consists of an optical fiber, one end of which is mechanically sharpened and coated with metal, having a small aperture of

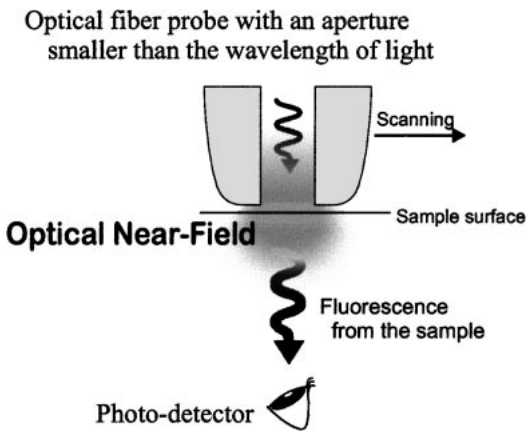


Fig. 8. Schematic drawing of an optical fiber tip and optical near-field at the surface of specimen.

less than 100 nm in diameter.[49,50] The light from various laser sources is coupled into the fiber at the other end, and then transmitted, confined, and finally emanated from the sharpened counter end which acts as a probe tip of the microscope. Figure 8 shows a schematic illustration of the probe tip.

As is true for other probe microscopes, the fiber tip is raster-scanned on the surface. Near-field light from the tip illuminates the surface of object only in a limited space. The intensity of fluorescence, resulting from the sample at the pointed area, is recorded by a conventional photon counting apparatus as a function of xy-coordinates. Thus, the mapping provides an optical image of fluorescence like a fluorescence microscope, together with the topography of the specimen. Light is not focused by a lens, but by the aperture of the fiber tip; therefore, this microscope does not suffer from the diffraction limit of light, resulting in a high spatial resolution of nanometer dimensions.

SNOM possesses many fascinating characteristics since it is operated by light. This means that the optical microscopy and fluorescence spectroscopy are combined with this novel apparatus, in other words, all of the benefits of the fluorescence method are available in this microscopy. Not only imaging, but also time-resolving, highly sensitive, and spectroscopic analyses are possible in the nanometric area of the specimen. Thus, the fluorescence probe method has a lateral resolution in a nanometer scale and will be further extending its applicability to materials technology and science.

**3.2. Imaging of a Single Polymer Chain in a Polymer Monolayer.** In this section, we will discuss the morphology of a single polymer chain embedded in a polymer monolayer. The use of SNOM allowed one for the first time to obtain the real image of a single chain existing in a polymer film. It is always fascinating and interesting for many polymer scientists to investigate individual chains. Many studies by STM and AFM, both scanning probe microscopes, have already shown the morphology of isolated chains adsorbed on a flat surface like a mica sheet.[51,52] However, SNOM is able to depict in situ features of polymer chains locating inside the polymer film, because near field light from the tip penetrates under the surface and shines selectively on the labeled single chains dispersed among large number of identical non-labeled chains of the matrix.[53]

Figure 9 depicts chemical structures of sample polymers. Poly(isobutyl methacrylate) (PiBMA) was employed for a base polymer of ultrathin film, because it is known to form a stable monolayer on the water surface with a thickness of 1 nm.[54] Besides the homopolymer, we prepared a labeled PiBMA (PiBMA-Pe) by means of copolymerization of isobutyl methacrylate and 3-perylenylmethyl methacrylate. As shown in Fig. 9, the copolymer bears perylene (Pe) chromophores at the side chain, whose fraction was suppressed to ca. 1% in order to avoid the influence of labels on the morphology of the polymer chain. Even for the small amount of labels, the fluorescence signal from single polymer chains could be recorded under the microscope. In Fig. 9, the molecular weight and its dispersion are also given both for labeled and for non-labeled PiBMA. We synthesized high molecular weight polymers in the order of $10^6$ so that they have an area large enough to be observable under the microscope with a resolution of 100 nm.

The films for SNOM measurements were prepared by the LB technique. Figure 10 shows the layer structure used in this

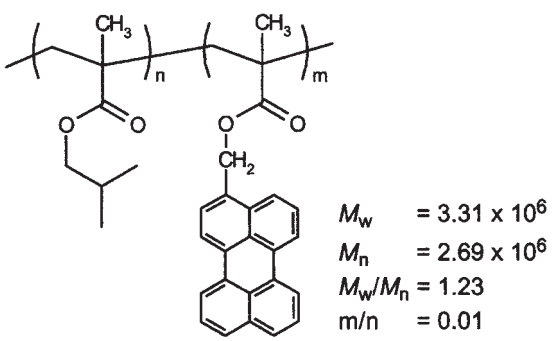


Fig. 9. Chemical structure of poly(isobutyl methacrylate) (PiBMA) and perylene chromophore labeled at the side chain.

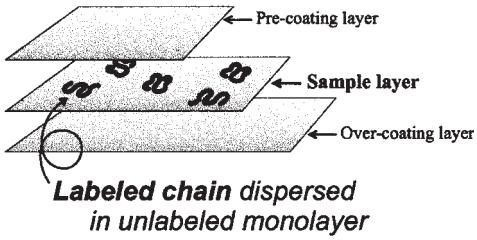


Fig. 10. Structure of ultrathin polymer films prepared for single chain observation by SNOM.

study. A very small quantity of PiBMA-Pe was embedded only in the middle layer of the PiBMA homopolymer and was sandwiched in between protecting layers of PiBMA. The near field light from the probe tip selectively excites the Pe dyes attached to the labeled PiBMA-Pe chains that constitute a part of the 2-dimensional monolayer film.

Figure 11(a) shows a SNOM image for PiBMA thin films containing the labeled polymers with a dilution of 1/700, i.e., the fraction $F$ of PiBMA-Pe in the PiBMA monolayer was adjusted to 0.14%. This picture was taken using the intensity of perylene fluorescence under the excitation at 442 nm (He–Cd laser wavelength). Several small spots like stars in the night sky were observed in the picture, although the surface was very flat over the whole area of the topographic images taken at the same time. Figure 11(b) shows another SNOM image for the sample with a dilution of 1/500. As the fraction $F$ was gradually increased, the number of spots also increased. This suggests that each spot corresponds to a single chain incorporated into the monolayer, but more quantitative evidence

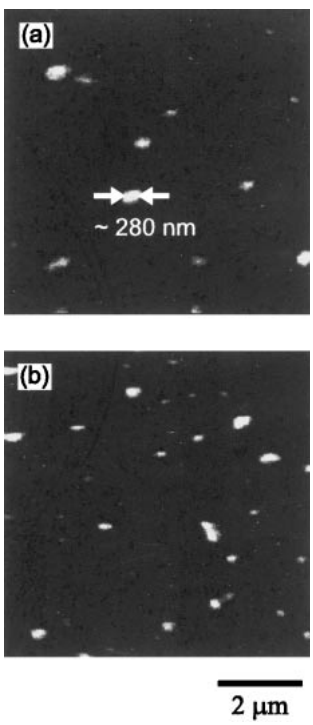


Fig. 11. SNOM image of single polymer chains observed by the intensity profile of fluorescence from perylene labels in a monolayer: (a) $F = 0.14\%$, (b) $F = 0.20\%$. The excitation wavelength was 442 nm.

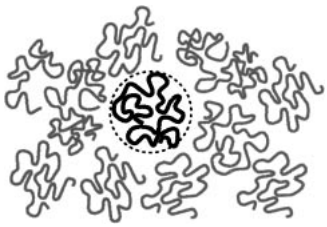

Fig. 12. Illustration for a contracted form of a polymer chain embedded in a two-dimensional monolayer film.

was highly desirable to support this speculation. Fortunately, we are able to evaluate the surface area $A$ of the monomer unit and the degree of polymerization $D_p$ from the molecular weight. Therefore, the plane density $\rho$ of PiBMA-Pe chain is simply given as:

$$\rho = F/(AD_p) \quad (8)$$

where $(AD_p)$ represents the area occupied by a single PiBMA-Pe chain. As for the sample in Figure 11(a), the plane density observed was 0.27 on average, and the density calculated by Eq. 8 was 0.28. This good agreement of the observed data confirms that each spot in these pictures represents a single chain embedded in the monolayer.

The size of spots is important. Some are large, and some are small. Obviously they have variations in both size and brightness. However, most spots have diameters around 200–300 nm in FWHM of the line profile. Considering the instrumental spatial resolution of ca. 100 nm, the real diameter of fluorescent area is estimated to be ca. 200 nm. Figure 12 shows a schematic illustration of polymer chain morphology as a reasonable explanation for the present system. The labeled polymer has a very large molecular weight, that is, a very long contour length of 8000 nm. However, from the area occupied by a single PiBMA-Pe chain, the diameter was estimated as only 110 nm, provided each chain takes a contracted form like a circle. Taking into account this value for a single chain, one may safely say that the polymer chains in 2-dimensions prefer the contracted conformations as shown in Fig. 12, because they cannot be entangled with other chains and have to exclude each other in order to avoid making free areas in plane. Although this behavior has been predicted by De Gennes' scaling theory[55] and also by our surface viscosity experiments,[56,57] the SNOM measurements provided unambiguous evidence for the first time thanks to the real images of fluorescence.

**3.3. Phase Separation Structure of Two-Dimensional Polymer Blends.** So far there is abundant information on 3-dimensional bulk polymers, but very little on 2-dimensional systems. The restricted space in reduced freedom may give rise to unexpected properties and structure of molecules. Therefore, many research projects have been aimed at nanomaterials having low dimensionality. The phase separation morphology of 2-dimensional monolayer of polymer blends is a major concern of the present section. Although the morphology of polymer blends in bulk systems has been extensively studied because of the improved mechanical and thermal characteristics compared with single component polymers, no work on 2-dimensional morphology for polymer blend and its phase separated structure has been reported, to the best of our knowledge.

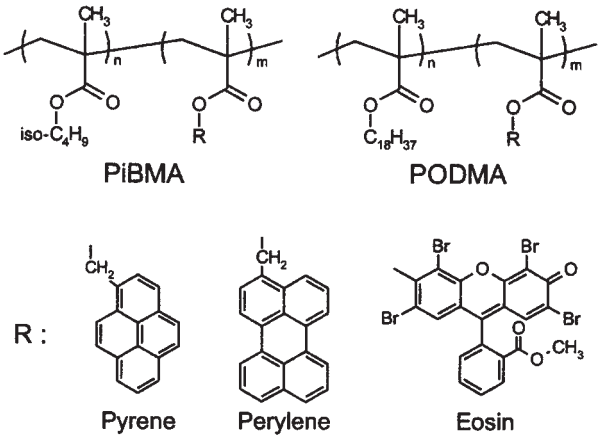


Fig. 13. Chemical structures of PiBMA and poly(octadecyl methacrylate) (PODMA). Fluorescent probes (R) were labeled at the side chain of each polymer separately.

In this study, we employed again PiBMA as one component of the monolayer, and poly(octadecyl methacrylate) (PODMA) as the other component.[58–60] The former gives a liquid like monolayer on the water surface, but the latter behaves as a solid-like monolayer due to the strong cohesive force among the long alkyl side chains.[61] Figure 13 illustrates the chemical structures of the polymers. PiBMA and PODMA were labeled separately with pyrene (Py), perylene, and eosin (Eo) dyes, which were appropriate pairs for energy transfer experiments as a donor and an acceptor. The mixed solution of PiBMA and PODMA was spread on the air/water interface at room temperature. The monolayer on the surface was compressed, and then transferred onto a quartz substrate. The crystalline side chain of PODMA starts melting on water at ca. 34 °C, and the monolayer alters the character to a liquid-like one. Therefore, the phase separation proceeds very fast at 40 °C, yielding a completely separated monolayer of the polymer blend.[61] We prepared samples deposited on substrates after various annealing periods at 40 °C.

Figure 14 shows three pictures of the PiBMA-Py/PODMA-Pe blend monolayer annealed for 1 h; these were taken by SNOM with three different excitation and monitoring wavelengths: the left picture is the fluorescence image of pyrene, which was selectively excited at 325 nm and observed at 370–410 nm; the middle is for perylene excited at 442 nm and detected at wavelengths longer than 470 nm. Obviously the bright part of the left picture indicates the presence of a PiBMA monolayer, and the bright area of the middle one corresponds to the PODMA monolayer. These two pictures perfectly complement each other, indicating that the phase separation took place completely, and that the surface was covered firmly by one of them, without any cracks or defects at all.

More interesting is the right picture in Fig. 14, which was taken by excitation of Py at 325 nm and by monitoring Pe fluorescence at wavelengths longer than 470 nm. Under this experimental condition, Pe was not excited by 325 nm light, and Py fluorescence could not be detected even if Py was excited. So, the fluorescence signal from Pe used for this

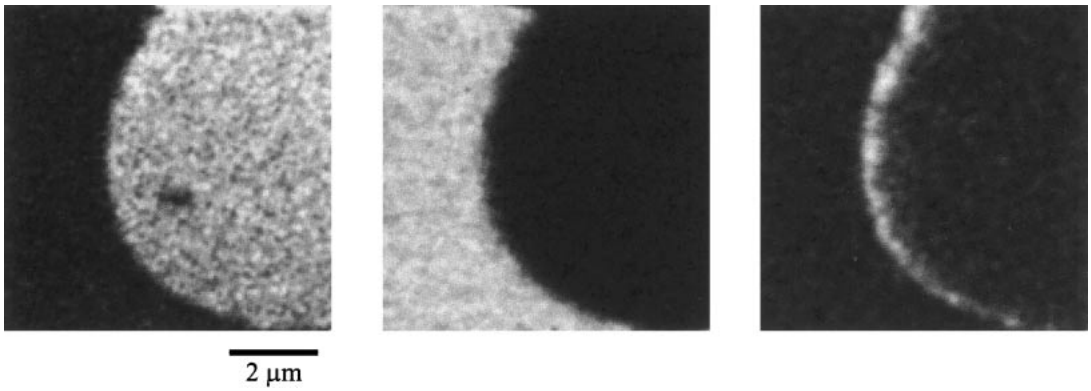


Fig. 14. Fluorescence SNOM images for the PiBMA-Py/PODMA-Pe phase separated monolayer. Left: Py fluorescence picture taken by excitation at 325 nm (Py), middle: Pe fluorescence image taken by excitation at 442 nm, right: energy transfer image resulting from Pe emission excited at the Py absorption band of 325 nm.[60]

imaging was emitted only through the energy transfer from Py to Pe. This means that the bright area in the right picture indicates the area in which PiBMA-Py/PODMA-Pe were molecularly mixed and approached each other within the Foerster radius (critical energy transfer radius) of around a few nanometers. In other words, the energy transfer mapping by SNOM could show up just the boundary of two domains as a result of indication of molecular mixing.

This energy transfer imaging showed the width of the boundary region to be about 300 nm, which is more than ten times the width for a 3-dimensional phase separation. Although the observed width is given by convolution of the real width and spatial resolution of the microscope, it is surely larger than that of 3-dimensional systems.

The enlargement of the boundary width was confirmed again by energy transfer experiments using point-by-point analysis of the fluorescence decay curves. The samples used in this experiment were PODMA-Pe as the donor and PiBMA-Eo as the acceptor. The Eo dyes of the latter component quench the excited state of the former Pe through the energy transfer mechanism. The closer the mutual distance of these two dyes, the faster the rate constant of quenching is. Therefore, the decay rate of Pe fluorescence reflects the local concentration of Eo dyes at the observed point. Figure 15 depicts the line profiles across the boundary of PODMA/PiBMA as indicated by the solid line in the upper picture; the fluorescence intensity and lifetime of Pe emission are plotted against the position of every 100 nm over the whole length of the boundary region. As the observed position is moved from the PODMA phase to PiBMA phase, both the fluorescence intensity and the lifetime of donor Pe decrease steeply, showing a rapid increase of the concentration of PiBMA-Eo. The intensity of fluorescence is usually proportional to the number of donor Pe under the scope, but the lifetime measurements directly manifest the alteration of local concentration of Eo chromophores at the specific point. Therefore, the lifetime profile provides unambiguous indication for the gradient of polymer composition across the boundary of the domains. These experiments show the high potential of the energy transfer method for the structural analysis, when it is combined with nanometric microscopy.

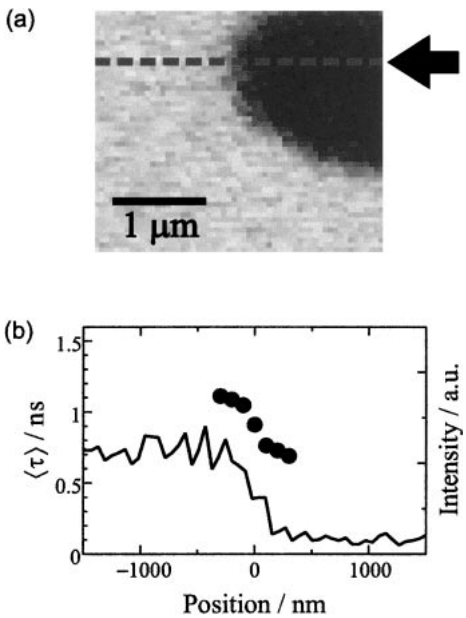


Fig. 15. (a) SNOM image for the PODMA-Pe/PiBMA-Eo recorded with fluorescence of Pe. (b) Line profiles of the fluorescence intensities (solid line) and the average lifetimes (circle) at positions across the phase-separated boundary indicated by the broken line in (a).[59]

**3.4. Inhomogeneous Network Structure of a Polymer Gel.** Polymer gels are made up of a 3-dimensional network of interpenetrating polymer chains. So far, many researchers have investigated the network structure using X-ray and light scattering measurements in order to clarify the origin of the unique and particular properties. However, the microscopic images of polymer gels in real space have been reported only for resolutions in larger than micrometer order using optical and scanning laser microscopy,[62,63] whereas polymer gels are known to form fractal structures over a wide range of dimensions from nanometer to micrometer regions. In this section, we deal with a PMMA gel labeled with fluorescence probes such as Pe and Eo chromophores; we tried to take its nanometric pictures in order to clarify the nanometric inhomogeneity.[64]

The sample was prepared by radical copolymerization of MMA monomer with a small amount of 3-perylenylmethyl methacrylate as a fluorescent probe and ethylene glycol dimethacrylate as a cross-linker. The PMMA gel obtained was swollen again with MMA monomer and bulk polymerized in order to solidify the gel with the same kind of polymer chains. The sample piece for SNOM observation was prepared from the thus obtained solid gel, which was sliced by a microtome, yielding a very thin film with a thickness of ca. 100 nm, and then the inner structure was observed by SNOM.

Figure 16 shows two pictures taken in different SNOM modes. The upper one (a) is the topographic picture, in which the oblique lines display scratch of the surface made by the knife edge of the microtome. However, the lower picture (b) of Fig. 16 was imaged by fluorescence of Pe probe at the same position as the upper one. No oblique lines appeared; instead, inhomogeneous distribution of intensity was observed with a size of 500–600 nm, suggesting the network structure of the PMMA gel. These pictures indicate that SNOM can be used to show the nano-structures inside the sample film, whereas AFM gives topographic images of the surface. A series of experiments using various gel samples confirmed that the inhomogeneous picture taken by the fluorescence mode represented the fluctuation of segment density of polymer chains, although the fluorescent probes were introduced into the polymer chains with a constant fraction.

The energy transfer method was also employed for the gel samples, and combined with the SNOM experiments. Perylene and eosin dyes are introduced into the PMMA chains in the gel; the latter dye eosin acts as an energy acceptor for the perylene donor. Figure 17(a) shows again an inhomogeneous structure of PMMA gel, in which the marked positions A and B were examined by the time-resolving measurement for perylene fluorescence with selective excitation at 415 nm light from the picosecond laser system. As discussed in the previous section, fluorescence decay analysis allows one to evaluate the concentration of acceptors around the donor molecule, because the energy transfer rate reflects the separations between the donor and acceptor probes. This analysis was performed at the points A and B marked in Fig. 17(a). As shown in Fig. 17(b), curves A and B, the decay functions at these points obviously consist of multi-component functions, but the average lifetimes are far shorter than the intrinsic decay function of the isolated perylene in a spin-cast film, which is plotted with the line D in Fig. 17(b). For comparison, we also prepared a control PMMA sample labeled by both perylene and eosin dyes with the same concentrations as the gel, but homogeneously distributed in the bulk, in order to evaluate the mean segment density through the energy transfer method. The decay shown in Fig. 17(b), curve C, is very similar to curve D for the isolated Pe. These results indicate that the PMMA gel has local segment densities 10 times higher than the homogeneous distribution.

Surprisingly, the fast decay rate, i.e., the high segment density, was almost constant irrespective of the positions observed. As seen in Fig. 17(a), the point A is much brighter than the point B, i.e., suggesting that the segment density at the A point is higher than that at the B point. However, the energy

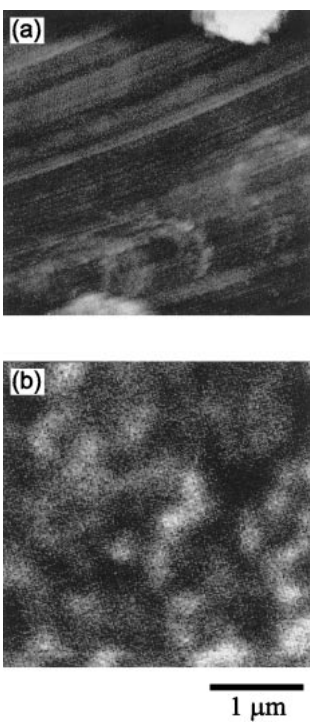


Fig. 16. (a) Topographic image of the surface of a PMMA gel sample. (b) SNOM image taken by the Pe fluorescence in the same area as (a). The excitation wavelength was 442 nm.[64]

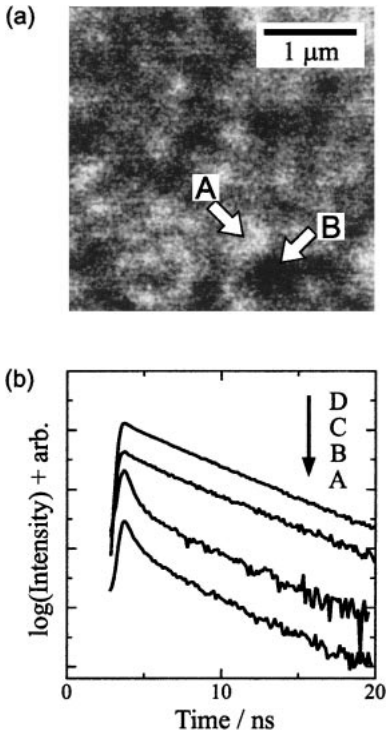


Fig. 17. (a) Fluorescence SNOM image of a PMMA gel labeled with Pe and eosin dyes. (b) Decay curves of Pe fluorescence observed for: (curves A and B) PMMA gel at points A and B indicated in (a), respectively, (C) PMMA bulk sample without cross-linker, (D) spin-cast film containing Pe chromophore.[64]

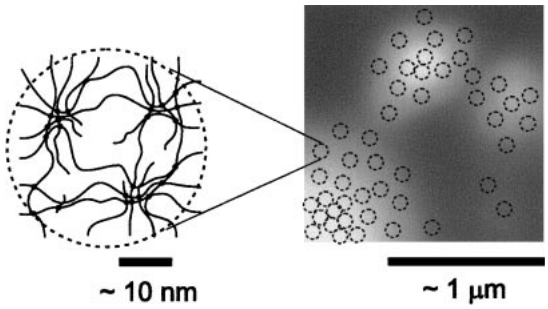


Fig. 18. A model of inhomogeneity observed by the fluorescence decay method (left) and the sub-micron inhomogeneity formed by aggregation of clusters, observed by the fluorescence SNOM image (right).[64]

transfer experiment obviously indicates that the density is independent of the observed position. This discrepancy can be explained by assuming a structural hierarchy of PMMA gel as schematically illustrated in Fig. 18. In the molecular scale of 1–10 nm, the network chain forms a micro-cluster, in which the chain segment is locally concentrated due to the introduction of cross-linking. Energy transfer take place between molecules closer than ca. 10 nm, the fluorescence decay function indicates this local environment of micro-cluster. In the larger scale of 10–1000 nm, the clusters are connected, and form aggregates with an inhomogeneous structure, which was observed by the fluorescence SNOM. Therefore, the dark and bright parts of SNOM image represent simply the small and large numbers of clusters, respectively, and the local concentration of polymer segment in molecular level is always very high, regardless of the brightness of the SNOM image. These experiments manifest the characteristics of the fluorescence probe method, which provides information of the structure and environment in a molecular scale.

## 4. Concluding Remarks

Light absorption and fluorescence phenomena result from direct interaction between molecules and photons, the latter propagating with information of the individual molecules. The fluorescence probe method utilizes the unique and particular characteristics of optical measurements. Spectroscopic and polarization analyses for selectively labeled molecules can be performed with extremely high sensitivity and ultra-fast time-resolution in air atmosphere. Although conventional types of optical microscopy such as fluorescence microscopy and confocal laser scanning microscopy fully possess these advantages of optical measurements, SNOM has brought further improvement in the spatial resolution, and has extended the applicability of optical microscopy to nanometer dimensions. Since SNOM is still in its infancy, novel ideas and techniques are continuously proposed, some of which steady improve the ability of this apparatus year by year. For example, some manufacturers provide a probe tip made from a cantilever of AFM. The incident light is focused into a hole made on the back of the cantilever, and the near-field emanates from the top of it. This type of SNOM probe has a high throughput of the incident light compared to that of the fiber type, and realizes higher lateral resolutions of ca. 30 nm, which is at least one order higher than the resolution of conventional optical microscopes. Using one of the advantages of the optical method, some research groups have reported observations in water because there are strong requests for applying SNOM to biological materials. Although nanoscale science is now widely performed in many fields, major interest has been paid to organic materials and their assemblies. Apart from metals and ceramics, the nano-structure of organic and biological materials must be soft and dynamical by nature. Therefore, the fluorescence method is expected to contribute greatly to the science of these materials as a tool for "seeing molecular assemblies in nanometer dimensions".

## References

1 Y. Nishijima, *J. Macromol. Sci., Phys.*, **B8**, 389 (1973).
2 "Polymer Photophysics," ed by D. Phillips, Chapman and Hall, London (1985).
3 "Photophysics of Polymers," ed by C. E. Hoyle and J. M. Torkelson, ASC Ser. 358, Am. Chem. Soc. (1987).
4 "Near-Field Nano/Atom Optics and Technology," ed by M. Ohtsu, Springer, Tokyo (1998).
5 "Nano-Optics," ed by S. Kawata, M. Ohtsu, and M. Irie, Springer, Berlin (2002).
6 "An Introduction to Ultrathin Organic Films," ed by A. Ulman, Academic Press, San Diego (1991).
7 S. Ito and M. Yamamoto, "New Macromolecular Architechture and Functions," ed by M. Kamachi and A. Nakamura, Springer, Berlin (1996), pp. 127–136.
8 N. Sato, S. Ito, K. Sugiura, and M. Yamamoto, *J. Phys. Chem. A*, **103**, 3402 (1999).
9 H. Ohkita, H. Ishii, S. Ito, and M. Yamamoto, *Chem. Lett.*, **2000**, 1092.
10 H. Okita, T. Ogi, R. Kinoshita, S. Ito, and M. Yamamoto, *Polymer*, **43**, 3571 (2002).
11 S. Ito, K. Kanno, S. Ohmori, Y. Onogi, and M. Yamamoto, *Macromolecules*, **24**, 659 (1991).
12 M. A. Winnik and F. M. Winnik, *Adv. Chem. Ser.*, **236**, 485 (1993).
13 D. A. Vanden Bout, J. Kerimo, D. A. Higgins, and P. F. Barbara, *Acc. Chem. Res.*, **30**, 204 (1997).
14 J. Teetsov and D. A. Vanden Bout, *J. Phys. Chem. B*, **104**, 9378 (2000).
15 J. Hofkens, W. Verheijen, R. Shukla, W. Dehaen, and F. C. DeSchryver, *Macromolecules*, **31**, 4493 (1998).
16 X. Michalet and S. Weiss, *Compt. Rend. Phys.*, **3**, 619 (2002).
17 L. A. Deschenes and D. A. Vanden Bout, *J. Phys. Chem. B*, **105**, 11978 (2001).
18 N. Sato, Y. Ohsawa, S. Ito, and M. Yamamoto, *Polym. J.*, **31**, 488 (1999).
19 N. Sato, K. Sugiura, S. Ito, and M. Yamamoto, *Langmuir*, **13**, 5685 (1997).
20 J. Matsui, M. Mitsuishi, and T. Miyashita, *J. Phys. Chem. B*, **106**, 2468 (2002).
21 K. Ono, K. Ueda, T. Sasaki, S. Murase, and M. Yamamoto, *Macromolecules*, **29**, 1584 (1996).
22 J. Horinaka, S. Amano, H. Funada, S. Ito, and M. Yamamoto, *Macromolecules*, **31**, 1197 (1998).
23 M. D. Ediger, *Annu. Rev. Phys. Chem.*, **42**, 225 (1991).
24 M. Yamamoto, K. Ono, and S. Ito, "Solvents and Self-Organization of Polymers," ed by S. E. Webber, Kluwer Academic

Pub., Dordrecht (1996), pp. 479–498.
25 T. A. Smith, L. M. Bajada, and D. E. Dunstan, *Macromolecules*, **35**, 2736 (2002).
26 H. Aoki, J. Horinaka, S. Ito, M. Yamamoto, H. Katayama, M. Kamigaito, and M. Sawamoto, *Polym. J.*, **33**, 464 (2001).
27 C. J. Hawker, *Trends Polym. Sci.*, **4**, 183 (1996).
28 "Controlled Radical Polymerization," ed by K. Matyjaszewski, ACS Symposium Ser. 685, Am. Chem. Soc., Washington DC (1998).
29 J. P. S. Farinha, J. G. Spiro, and M. A. Winnik, *J. Phys. Chem. B*, **105**, 4879 (2001).
30 Y. Rharbi and M. A. Winnik, *Macromolecules*, **34**, 5238 (2001).
31 M. Suwa, A. Hashizume, Y. Morishima, T. Nakato, and M. Tomida, *Macromolecules*, **33**, 7884 (2000).
32 S. Yusa, A. Sakakibara, T. Yamamoto, and Y. Morishima, *Macromolecules*, **35**, 10182 (2002).
33 K. Iwai, K. Hanasaki, and M. Yamamoto, *J. Lumin.*, **87**, 1289 (2000).
34 T. Kanaya, K. Goshiki, M. Yamamoto, and Y. Nishijima, *J. Am. Chem. Soc.*, **104**, 3580 (1982).
35 S. Ito, M. Yamamoto, and Y. Nishijima, *Bull. Chem. Soc. Jpn.*, **55**, 363 (1982).
36 S. Ito, S. Oki, T. Hayashi, and M. Yamamoto, *Thin Solid Films*, **244**, 1073 (1994).
37 W. C. Tao and C. W. Frank, *Macromolecules*, **23**, 3275 (1990).
38 R. Xie, B. Yang, and B. Jiang, *Polymer*, **34**, 5016 (1993).
39 G. Liu and J. E. Guillet, *Macromolecules*, **23**, 1388 (1990).
40 G. Liu, *Macromolecules*, **26**, 1144 (1993).
41 Th. Foerster, *Z. Naturforsch., A: Phys. Sci.*, **4**, 321 (1949).
42 S. Ohmori, S. Ito, and M. Yamamoto, *Macromolecules*, **24**, 2377 (1991).
43 M. Watanabe, Y. Kosaka, K. Oguchi, K. Sanui, and N. Ogata, *Macromolecules*, **21**, 2997 (1988).
44 S. Ohmori, S. Ito, M. Yamamoto, Y. Yonezawa, and H. Hada, *J. Chem. Soc., Chem. Commun.*, **1989**, 1293.
45 M. Yamamoto, K. Kawano, T. Okuyama, T. Hayashi, and S. Ito, *Proc. Jpn. Acad., Ser. B*, **70**, 121 (1994).
46 T. Hayashi, T. Okuyama, S. Ito, and M. Yamamoto, *Macromolecules*, **27**, 2270 (1994).
47 M. Mabuchi, K. Kawano, S. Ito, M. Yamamoto, M. Takahashi, and T. Masuda, *Macromolecules*, **31**, 6083 (1998).
48 S. Ito, K. Kawano, M. Mabuchi, and M. Yamamoto, *Polym. J.*, **28**, 164 (1996).
49 T. Saiki, S. Mononobe, M. Ohtsu, N. Saito, and J. Kusano, *Appl. Phys. Lett.*, **68**, 2612 (1996).
50 S. Mononobe, T. Saiki, T. Suzuki, S. Koshihara, and M. Ohtsu, *Opt. Commun.*, **146**, 45 (1998).
51 J. Kumaki, Y. Nishikawa, and T. Hashimoto, *J. Am. Chem. Soc.*, **118**, 3321 (1996).
52 J. Kumaki and T. Hashimoto, *J. Am. Chem. Soc.*, **120**, 423 (1998).
53 S. Ito, H. Aoki, and M. Anryu, *Trans. MRS-J*, **26**, 929 (2001).
54 K. Naito, *J. Colloid Interface Sci.*, **131**, 218 (1989).
55 P. G. DeGennes, "Scaling Concepts in Polymer Physics," Cornell University, Ithaca, N.Y. (1979).
56 N. Sato, S. Ito, and M. Yamamoto, *Polym. J.*, **28**, 784 (1996).
57 N. Sato, S. Ito, and M. Yamamoto, *Macromolecules*, **31**, 2673 (1998).
58 H. Aoki, Y. Sakurai, S. Ito, and T. Nakagawa, *J. Phys. Chem. B*, **103**, 10553 (1999).
59 H. Aoki and S. Ito, *J. Phys. Chem. B*, **105**, 4558 (2001).
60 H. Aoki, Y. Kunai, S. Ito, H. Yamada, and K. Matsushige, *Appl. Surf. Sci.*, **188**, 534 (2002).
61 Y. Sakurai, N. Sato, S. Ito, and M. Yamamoto, *Kobunshi Ronbunshu*, **56**, 850 (1999).
62 Y. Hirokawa, H. Jinnai, Y. Nishikawa, T. Okamoto, and T. Hashimoto, *Macromolecules*, **32**, 7093 (1999).
63 H. Jinnai, H. Yoshida, K. Kimishima, Y. Funaki, Y. Hirokawa, A. E. Ribbe, and T. Hashimoto, *Macromolecules*, **34**, 5186 (2001).
64 H. Aoki, S. Tanaka, S. Ito, and M. Yamamoto, *Macromolecules*, **33**, 9650 (2000).

Shinzaburo Ito was born in January of 1951 in Shiga, Japan. In 1973, he graduated from Kyoto University (Department of Polymer Chemistry) and finished the graduate school of Kyoto University in 1978. He obtained his doctoral degree of Engineering (Polymer Chemistry) in 1981 from Kyoto University with a thesis on "Studies on Intramolecular Excimer Formation in Polymer Systems". He was appointed as a Research Instructor of Kyoto University in 1979. He experienced being a guest scientist of Max-Planck Institute for Polymer Research (Mainz) in the laboratory of Prof. W. Knoll from 1991 to 1992, and was also a visiting research fellow of RIKEN (Wako) during 1993–1999. He was promoted to Associate Professor in 1994 and to Professor of Department of Polymer Chemistry, Kyoto University, in 1999. His research interest encompass the polymer nano-structure, polymer photophysics and photochemistry, ultra-thin films and their optical and electrical properties.

Hiroyuki Aoki was born in April of 1973. He graduated from the Department of Polymer Chemistry of Kyoto University in 1996. In 2001, he received his degree of Dr. of Engineering from Kyoto University with a thesis on "Nanometric Structures and Nanosecond Dynamics of Ploymers Studied by Fluorescence Methods". He experienced being a post-doctoral fellow in the Department of Electronic Science and Engineering, Kyoto University from April to September in 2001. He has been a Research Associate of the Department of Polymer Chemistry, Graduate School of Engineering, Kyoto University since October of 2001. His research interests are focused on the polymer nano-structure and near-field optics.